Research Article

Ambrož Kregar* and Tomaž Katrašnik

Theoretical analysis of particle size re-distribution due to Ostwald ripening in the fuel cell catalyst layer

https://doi.org/10.1515/phys-2019-0081
Received Jul 30, 2019; accepted Sep 17, 2019

Abstract: The limited durability of hydrogen fuel cells is one of the main obstacles in their wider adoption as a clean alternative technology for small scale electricity production. The Ostwald ripening of catalyst material is recognized as one of the main unavoidable degradation processes deteriorating the fuel cell performance and shortening its lifetime. The paper systematically studies how the modeling approach towards the electrochemically driven Ostwald ripening in the fuel cell catalyst differs from the classical diffusion driven models and highlights how these differences affect the resulting evolution of particle size distribution. At moderately low electric potential, root-law growth of mean particle size is observed with linear relation between mean particle size and standard deviation of particle size distribution, similar to Lifshitz-Slyozov-Wagner theory, but with broader and less skewed distribution. In case of high electric potential, rapid particle growth regime is observed and qualitatively described by redeposition of platinum from a highly oversaturated solution, revealing the deficiencies of the existing platinum degradation models at describing the Ostwald ripening in the fuel cells at high electric potentials. Several improvements to the established models of platinum degradation in fuel cell catalysts are proposed, aimed at better description of the diffusion processes involved in particle growth due to Ostwald ripening.

Keywords: Fuel cell, Ostwald ripening, modeling, theory, platinum degradation

PACS: 68.35.Fx, 68.43.Jk, 68.55.A, 81.10.Dn

***Corresponding Author: Ambrož Kregar:** Institute of Physical and Theoretical Chemistry, Graz University of Technology & Faculty of Mechanical Engineering, Universtity of Ljubljana; Email: ambroz.kregar@fs.uni-lj.si

Tomaž Katrašnik: Faculty of Mechanical Engineering, Universtity of Ljubljana; Email: tomaz.katrasnik@fs.uni-lj.si

1 Introduction

The increased concerns with environmental issues calls for the radical changes in human energy management. The transport sector, being one of the primary sources of carbon dioxide emissions, is facing a dramatic transformation from traditional means of propulsion, based on internal combustion engines, towards cleaner and more energy efficient electric motors, powered by either batteries or hydrogen fuel cells [1]. Although the battery powered vehicles are currently more widely spread [2], short refuelling times and long ranges, approaching the ones of conventional internal combustion engine powered vehicles characterizes fuel cell vehicles as a viable solution for frequently used long range vehicles [3]. Low temperature polymer membrane fuel cells (LT-PEMFC), most often used in road vehicles, produce electricity by combining hydrogen and oxygen into water through a pair of redox reaction on two catalyst layers, separated by a polymer membrane, functioning as a proton conductor. The increased temperature and humidity, heterogeneous electric potential and presence of multitude of reactive species in the fuel cell leads to a severe degradation of the catalyst layer, typically composed of Pt nanoparticles, deposited on a highly porous carbon support. Several degradation mechanisms affect the catalyst layer during fuel cell operation, leading to the growth in Pt particle size and consequential decrease in useful electrochemical surface area. In addition to carbon corrosion and consequent Pt detachment from carbon support, the Pt dissolution is among the most prominent degradation processes. Not only does it lead to the diffusion of Pt ions into the fuel cell membrane, initiating its chemical degradation, the local redeposition of Pt from smaller to larger particles, the so-called Ostwald ripening, plays an important role in the structural changes of the fuel cell catalyst.

The process of Ostwald ripening was first observed and described by Wilhelm Ostwald in 1901 [4] and denotes a process of coarsening of the particles, dispersed in a matrix and interacting via shared reservoir of dissolved ma-

terial [5]. The process is driven towards the decrease in total surface free energy of the particles. The surface energy of particles depends on their size, as described by Gibbs-Thompson equation [5]

$$C_r = C_e \exp\left(\frac{r^\star}{r}\right), \tag{1}$$

relating the equilibrium concentration at the surface of the particle C_r to the equilibrium concentration above a flat surface C_e, and the particle radius r, with capillarity length $r^\star = \frac{2\sigma M}{RT}$ being determined by surface tension σ, molar mass M, general gas constant R and temperature T. This size dependence of equilibrium potential leads to dissolution of particles below some critical size and redeposition of dissolved material on larger particles [5].

The process was first mathematically described by Lifshitz and Slyozov [6] and later by Wagner [7] in the so-called Lifshitz-Slyozov-Wagner (LSW) theory [5]. The authors assumed the particles in distribution to be sufficiently larger than capillarity length $r^\star$ to justify the expansion of exponent in (1) to a linear term in $1/r$, and also infinitesimally small ratio between volumes of solid and dissolved phase. This allows for analytic solution for both, the time dependence of the mean size of the particles in the system and the shape of particle size distribution (PSD), which will be explained in more detail in Section 2.1.

Ostwald ripening was subsequently studied by many authors, introducing the effects of finite ratio between solid and dissolved phase [8] and improving the methods to describe interparticle diffusion [9], particle encounters [10] and diffusion properties in coarsely-grained environment [11]. The importance of difference in processes limiting the material transfer between particles was highlighted by Slezov [12] and more recently by Myers [13]. The generalized theoretical approach for various mass-transfer mechanisms was provided by Alexandrov [14], along with the detailed study of the effect of Ostwald ripening before the PSD approaches the asymptotic regime [15]. It is important to note that all listed approaches result in the same asymptotic form of mean particle size growth as LSW theory, with the growth rate parameter taking different values, depending on the details of the system in consideration. While the general scaling properties of the PSD are conserved in different models, the standard deviation and skewness strongly depend on the modelling approach.

Despite the great variety of approaches, the models typically consider the system of particles in metal alloys [5], where mean particle size is considerably larger than capillarity length $r >> r^\star$ and the dissolution of particles is driven only by the difference between the chemical potential on the particles surface and in the interparticle solution. These approaches, however, are not applicable to the Ostwald ripening in fuel cell catalyst layer. Firstly, since the particle sizes in modern Pt catalyst are in the range of only a few nanometers, the full exponential form of Gibbs-Thompson relation (1) needs to be taken into account. Even more importantly, the dissolution mechanism in fuel cell catalyst is essentially an electrochemical process, forced by electric potential, which leads to some important differences in the dissolution kinetics [16] compared to the approaches listed in previous paragraph.

The models of size-dependent electrochemical dissolution in the catalyst are included in many fuel cell degradation models, describing Pt dissolution [16], migration [17] and redeposition [18]. The degradation models were used to analyze the changes of PSD in fuel cell catalysts due to Ostwald ripening [19] with some also adding the effects of particle agglomeration [20] and size-dependent oxide coverage of particles [21]. The differences between standard models of Ostwald ripening [5] and Ostwald ripening in electrochemical systems [18], however, have never been systematically addressed at the level of general properties of PSD and growth rate.

The aim of this study is to highlight the differences between the properties of Ostwald ripening in standard modelling approaches and Ostwald ripening in fuel cell catalyst layer. This is done by establishing a mean-field model of Ostwald ripening, based on established models of Pt dissolution in the fuel cell catalyst layer (e. g. [17, 20, 21]), solving it numerically and comparing the results with the predictions of LSW theory. Although not the most sophisticated of Ostwald ripening theories, LSW theory was chosen due to the simplicity of its assumptions and results, clearly highlighting the important differences between standard and electrochemically based models of Ostwald ripening [5]. The comparison was focused on the time dependence of mean particle size and the relations between moments of PSD, namely mean particle size, standard deviation and skewness [22]. The results indicate that the difference in dissolution mechanisms indeed leads to the significant differences in the shape of PSD. Even more importantly, the study reveals some potential deficiencies of established models of Ostwald ripening in electrochemical systems, such as the lack of diffusion effects, which might be an important factor in the improvement of existing fuel cell degradation models.

2 Model

The aim of this section is to present the underlying assumptions of classical model of Ostwald ripening [5] and compare them with the Ostwald ripening models used in electrochemical systems. The most important differences between the models will be highlighted and the numerical methods used to study the electochemical Ostwald ripening will be presented.

2.1 Classical model of Ostwald ripening

Standard Ostwald ripening model, used as a basis of LSW theory [5, 6], assumes the changes in particle size due to dissolution and redeposition based on equation

$$\frac{dr}{dt} = \frac{D}{r}\left(\Delta - \frac{\alpha}{r}\right), \tag{2}$$

with $\Delta = c - c_\infty$ being small difference between current (c) and saturated concentration (c_∞). D denotes the diffusion constant and $\alpha = 2\sigma v c_\infty/(RT)$ is determined by surface tension σ and atomic volume of the solute v, solubility c_∞, gas constant R and temperature T [6]. The bracketed term describes the effects, originating from Gibbs-Thompson equation (1), expanded for large r, while the size dependent factor D/r describes the diffusion of solute close to the particle surface under assumption that equilibrium concentration c_∞ is reached infinitely far from the particle.

According to (2) the particles with radius smaller than some limit value $r_L = \alpha/\Delta$ will be dissolving while larger partilces will be growing. The particle size re-distribution resulting from this mechanism is calculated as [5]

$$\frac{\partial f(r,t)}{\partial t} = -\frac{\partial}{\partial r}\left[\dot{r}(r) f(r,t)\right], \tag{3}$$

with $f(r,t)$ being PSD and particle growth rate (2) $\dot{r}(r) = \frac{dr}{dt}$.

Under the assumption $\Delta \ll c_\infty$, the asymptotic analytical solution for $t \to \infty$ for time dependence of mean particle size $\bar{r}(t)$ can be found, which obeys the equation

$$\bar{r}(t)^3 = r_0^3 + \beta t, \tag{4}$$

with $\beta = \frac{8\sigma c_\infty v^2 D}{9RT}$. What is important is that PSD $f(r,t)$ can also be expressed analytically as a function with specific scaling property

$$f(r) = g(r/\bar{r}(t)), \tag{5}$$

where

$$g(x) = \frac{81 e^{1-\frac{1}{1-\frac{2x}{3}}} x^2}{2^{5/3}\left(\frac{3}{2}-x\right)^{11/3}(x+3)^{7/3}}. \tag{6}$$

It is important to note that the same form of PSD $g(x)$ is retained during system evolution, with only parameter $x = r/\bar{r}(t)$ changing with time as determined by equation (4). These two important results of LSW theory will be used for comparison with Ostwald ripening in electrochemical system, given in Section 3.

The improvements of LSW model are typically applied by taking into account the finite volume fraction of condensed particles, decreasing the diffusion distance and therefore altering the diffusion dependant term D/r while keeping the dissolution part of the model the same. This results in modification of PSD (6), but retaining the same scaling property (5). The mean size growth of form (4) retains the same functional dependency with only parameter β being modified [5, 8].

2.2 Platinum dissolution and Ostwald ripening in electrochemical environment

The models of Pt dissolution and redeposition in electrochemical environment, used to describe the Ostwald ripening in fuel cell catalyst layer (e. g. [16, 20, 21]), assume that Pt particles are being dispersed on the carbon surface, providing good electron conductivity, and embedded in the ionomer matrix through which the dissolved Pt ions can diffuse. In contrast to standard Ostwald ripening, the Pt dissolution and redeposition in fuel cell catalyst proceeds via equilibrium electrochemical reaction [16]

$$Pt \leftrightharpoons Pt^{2+} + 2e^-, \quad E_{dis} = 1.188\text{V vs. RHE}. \tag{7}$$

On the flat surface, the reaction approaches equilibrium at reference concentration c_{ref} and potential difference $E_{dis} = 1.188\,\text{V}$ against reversible hydrogen electrode (RHE) [16]. Above a curved surface with radius of curvature r, the equilibrium potential is shifted according to Kelvin equation [16], derived from Gibbs-Thompson equation (1):

$$E_{dis}(r) = E_{dis} - \frac{\sigma M}{2F\rho}\frac{1}{r}. \tag{8}$$

The shift in equilibrium potential is determined by surface tension σ, molar mass M, solid phase density ρ and Faraday constant F.

When out of equilibrium, the reaction (7) proceeds in direct or reverse directions, depending on voltage U, resulting in Pt dissolution or redeposition. For the case of spherical particle, this results in its growth or shrinkage accord-

ing to equation [16]

$$\frac{dr}{dt} = -k_{dis}\frac{M}{\rho}\left[e^{\frac{\alpha n_e F}{RT}\left(U-E_{dis}(r)\right)} - \frac{c_{Pt^{2+}}}{c_{ref}}e^{-\frac{(1-\alpha)n_e F}{RT}\left(U-E_{dis}(r)\right)}\right]. \quad (9)$$

The number of transferred electrons during dissolution reaction is $n_e = 2$, while the reaction asymmetry $\alpha = 0.5$ is usually assumed in the literature [16, 17]. The expression (9) can therefore be further simplified to

$$\frac{dr}{dt} = -k_{dis}\frac{M}{\rho}\left[K_0(U)K_r(r) - \frac{c_{Pt^{2+}}}{c_{ref}}K_0^{-1}(U)K_r^{-1}(r)\right]. \quad (10)$$

with $K_0(U) = \exp\left(\frac{\alpha nF(U-E_{dis})}{RT}\right)$ describing the voltage-dependent part of dissolution rate and $K_r(r) = \exp\left(\frac{\alpha n\sigma M}{2\rho RTr}\right) = \exp\left(\frac{r_K}{r}\right)$ being size-dependent part.

One factor, affecting the dissolution rate but not taken into account in (9), is the coverage of Pt surface with stable oxide layer that passivizes the surface and therefore reduces the dissolution rate. This effects plays an important role in Pt dissolution during voltage cycling [23], but was in our case omitted to preserve the simplicity of the model and more clearly present only the most fundamental differences between classical and electrochemical Ostwald ripening.

For the case of Pt in the LT-PEMFC, operating at about 80°C, the characteristic radius is $r_K = \frac{\alpha n\sigma M}{2\rho RT} \approx 4.3$ nm [16]. Compared to typical particle size of $r \sim 2$ nm in modern fuel cell catalysts [24], we conclude that the full exponential form of size dependence $K_r(r)$ in (10) needs to be taken into account when describing Ostwald ripening in the fuel cell catalyst layer. By introducing a voltage dependent saturated equilibrium Pt concentration at the flat plane surface as

$$c_\infty(U) = c_{ref}K_0^2(U) \quad (11)$$

the dissolution rate can be further simplified to

$$\frac{dr}{dt} = \frac{r_K}{\tau(U)}\left(\frac{c_{Pt^{2+}}}{c_\infty(U)}K_r^{-1}(r) - K_r(r)\right), \quad (12)$$

where voltage dependent characteristic time was defined as

$$\tau(U) = \tau_0 K_0^{-1}(U) = \frac{\alpha n_e \sigma}{2RTk_{dis}}K_0^{-1}(U). \quad (13)$$

It is important to note that $\tau(U)$ decreases exponentially with increased voltage, and also depends on temperature T and dissolution rate $k_{dis} = 3.4\times10^{-9}$ mol m^{-2} s^{-1}, with its value taken from Ref. [16]. At equilibrium voltage $U = E_{dis,0}$ with $K_0 = 1$, the characteristic time $\tau_0 \approx 1.4\times10^5$ s $\approx$ 37 h, defining the time scale of system evolution.

The reaction rate (9) can be used to model the Ostwald ripening by assuming an ensemble of N particles of various sizes, distributed according to size distribution $f(r) = dN/dr$ with $N = \int f(r)dr$. In a mean-field model, proposed by Darling [16], all the particles in the ensemble are coupled to the same value of Pt concentration $c_{Pt^{2+}}$ in the interparticle space, with no non-uniformity or diffusion effects taken into account. This approach can to some extent be justified by the specific conditions in the fuel cell catalyst, with relatively small distances between particles ($d = \sqrt[3]{V_0/N} \sim 10$ nm where V_0 is the catalyst volume [24]) and large Pt diffusivity in the ionomer ($D_{Pt^{2+}} = 3.4\times10^{-11}$ m^2/s [17]), resulting in characteristic diffusion time $\tau_{dif} = \frac{d^2}{D_{Pt^{2+}}} \sim 10^{-6}$ s. Since this value is orders of magnitude smaller than τ_0, the omission of diffusion effects is a reasonable assumption.

Since particles of all sizes exchange the Pt ions with the shared reservoir, the time derivative of concentration $c_{Pt^{2+}}$ is determined by the integration over all particles in the distribution

$$\frac{dc_{Pt^{2+}}}{dt} = \frac{\rho}{MV_0}\int 4\pi r^2 f(r)\dot{r}(r)dr, \quad (14)$$

with $\dot{r}(r) = dr/dt$ being size dependent dissolution rate (9). V_0 represents the volume of interparticle space, available for dissolved Pt, which is considered to be constant in existing electrochemical Ostwald ripening models [20] as well as in LSW theory [5].

A pseudo steady-state Pt ion concentration $c_{Pt^{2+}}$, denoted c_S, can be determined by solving the equation (14) for $\frac{dc_{Pt^{2+}}}{dt} = 0$, resulting in

$$c_S = c_\infty(U)\frac{\int K_r(r)r^2f(r)dr}{\int K_r^{-1}(r)r^2f(r)dr} = c_\infty(U)F\left[f(r)\right], \quad (15)$$

where functional $F\left[f(r)\right]$ was introduced, with its value defined solely by the shape of PSD $f(r)$. Note that c_S is not a real steady-state value since even at this conditions, the PSD is changing and therefore also the Pt ion concentration. Similarly to classic Ostwald ripening model, the particles smaller than some limiting size r_L, determined as $\dot{r}(r_L) = 0$:

$$r_L = 2r_K \log F\left[f(r)\right], \quad (16)$$

will be dissolving and the dissolved Pt will be redeposited on particles larger than r_L. The time evolution of particle size redistribution due to Ostwald ripening in electrochemical system is governed by the same continuity equation (3) as in classical case, but with particle growth rate (9) being used.

2.3 Comparison between classical and electrochemical Ostwald ripening model

The expansion of electrochemical reaction rate (12) under assumption $r >> r_K$, $K_r(r) \approx 1 + \frac{r_K}{r}$. yields a result similar to (2):

$$\frac{dr}{dt} = \frac{r_K}{\tau(U)} \left(\tilde{\Delta}(U) - \frac{\tilde{\alpha}(U)}{r} \right), \tag{17}$$

where

$$\begin{aligned} \tilde{\Delta}(U) &= F\left[f(r)\right] - 1, \\ \tilde{\alpha}(U) &= r_K \left(F\left[f(r)\right] + 1 \right). \end{aligned} \tag{18}$$

Although the bracketed term in equation (17) is very similar in both cases, note that the expansion for small r_K/r is not justified in fuel cell catalyst with $r_K \sim 5\,\text{nm}$ is larger than mean particle size. The assumption of small $\tilde{\Delta}(U)$ can also hardly be justified, with $F\left[f(r)\right] \sim 1$ again being true only for large mean particle sizes $\bar{r}$. Both arguments clearly highlight the importance of the use of original electrochemical particle growth rate (9) in Ostwald ripening modeling in the fuel cell to obtain physically relevant results.

Also note that size dependent prefactor D/r in equation (2), is in equation (17) substituted by voltage dependent prefactor, indicating the differences in the origin of mass transfer mechanism between classical and electrochemical Ostwald ripening.

2.4 Numerical methods

To highlight the differences between cases of classical and electrochemically driven Ostwald ripening, the equations of electrochemical particle growth rate (9) was incorporated into equation for PSD (3) and Pt ion concentration evolution (14) and solved numerically by discretization of PSD: $f(r_i, t) \rightarrow f_i(t)$ and using symmetric finite difference method [25] to estimate the derivative of the product in the right hand side of the equation (3):

$$\begin{aligned} \dot{f}_i(t) = -\frac{1}{\Delta r} \Big[& \dot{r}(r_i) \left[f_{i+1}(t) - f_{i-1}(t) \right] + \\ & + f_i(t) \left[\dot{r}(r_{i+1}) - \dot{r}(r_{i-1}) \right] \Big] \end{aligned} \tag{19}$$

The range of particle sizes with discretization $\Delta r = 0.125\,\text{nm}$ was selected to be between $r_{min} = 0.125\,\text{nm}$ (to avoid divergence of dissolution rate at $r = 0$) and $r_{max} = 15\,\text{nm}$ (the largest particle size in aged fuel cell catalyst [26]). According to [6], the initial shape of PSD should play no role in asymptotic behaviour of the system and therefore a normal distribution of particles was assumed, with initial mean particle size $\bar{r}(0) = 2\,\text{nm}$ and standard deviation $\sigma(0) = 0.5\,\text{nm}$ [24]. In the absence of diffusion processes, the density of particles in the matrix should play no role in asymptotic system behaviour since equilibrium Pt concentration $c_{Pt^{2+}}$ is expected to retain its pseudo steady-state value (15). This assumption was tested by choosing three different initial particle densities: $n_A = 2.4 \times 10^{24}/\text{m}^3$ being typical density in real fuel cell catalyst, and smaller particle densities $n_B = 2.4 \times 10^{19}/\text{m}^3$ and $n_C = 2.4 \times 10^{14}/\text{m}^3$. Since the electric potential U plays an important role in effective Pt solubility in the ionomer (12), the whole range of potentials between 0 and 1.4 V, relevant in the fuel cell, was tested at each particle density. The integration times were chosen such that the mean particle size increased beyond the characteristic radius r_K, which is long enough for the PSD to evolve to its asymptotic shape.

3 Results and discussion

To highlight the differences between classical model of Ostwald ripening and electrochemical model, used in electrochemical systems, the results of LSW theory, presented in Section 2.1 will be compared with the results obtained by numerical simulation of electrochemical model, explained in Section 2.2. Several aspects of the model results will be compared: the time dependence of mean particle size, the properties of PSD, namely its standard deviation and skewness, and the robustness of the solution to the differences in initial conditions.

3.1 Particle growth rate - Ostwald ripening regime

The first system property of interest was the time evolution of mean particle size, calculated from numerically calculated distribution $f_i(t)$ as

$$\bar{r}(t) = \sum_i r_i f_i(t) / \sum_i f_i(t). \tag{20}$$

The results for all three particle densities n_A, n_B and n_C are plotted in Figure 1 for values of electric potential U between 0 and 1.4 V in an intervals of 0.05 V as a function of renormalized time $t' = t/\tau(U)$, scaled by voltage dependent characteristic time $\tau(U)$, defined in (13).

It can be seen from Figure 1 that for low voltages, the growth rates for all particle densities exhibit identical behaviour in renormalized time t', indicating that the growth

mechanism is identical in all cases. Furthermore, the results can be fitted perfectly with a model function, similar to (4)

$$\bar{r}^p(t') = \left(r_0^p + \beta'^p t'\right), \tag{21}$$

where p, r_0 and β' are fitting parameters. The black dotted line in Figure 1 shows the best fitted function, obtained at fitting parameters

$$r_0 = 2.19\,\text{nm}, \quad \beta' = 7.58\,\text{nm}, \quad p = 2.92 \tag{22}$$

The fitted exponent $p = 2.92$ indicates a very similar growth rate as for standard Ostwald ripening (4), where $p = 3$. The fitted initial radius $r_0 = 2.19\,\text{nm}$ takes a value reasonably close to the mean radius of initial distribution $\bar{r}(0) = 2\,\text{nm}$. Note that constant coefficient β' in renormalized time t' implies that growth coefficient $\beta = \beta'/\tau(U)$ in physical time t (see Eq. (4)) increases exponentially with the voltage U, which can be explained by increased solubility of Pt at elevated voltage (11), as suggested by LSW result, where β is proportional to solubility c_∞. The exact value of β' depends on other system parameters, but since it does not affect the general growth law, it was not further analyzed.

The growth profile of mean particle size in Figure 1 shows a close resemblance between classical and electrochemical Ostwald ripening. However, it can be further be discerned from Figure 1 that at increased voltages, the growth rate is drastically increased, indicated by almost instantaneous growth in mean particle size for large voltages. This indicates the particle growth mechanism notably different from Ostwald ripening, which will be further explored and analyzed in the next section.

3.2 Particle growth rate - high voltage regime

The process of fast, non-Ostwald particle growth at high voltage values, was further analyzed by plotting the mean particle size as a function of renormalized time t', with focus on short time scales, shown in Figure 2. The mean particle size in this regime shows exponential growth, with the growth rate increasing with voltage even in renormalized time scale. This behaviour is significantly different from classical Ostwald ripening and calls for more detailed explanation, which can on qualitative level be provided by the the relationship between saturated concentration of Pt c_S (15), electric potential U and mean particle size in the system (15).

For a system with narrow PSD where $\sigma \ll \bar{r}$ with mean particle size $\bar{r}$ at voltage U, the saturated particle concentration can, following equation (15), be approximated as

$$c_S \approx c_\infty(U) K_r^2(\bar{r}), \tag{23}$$

that is increasing with electric potential and decreasing with particle size. In standard Ostwald ripening regime, the increase in particle size and decrease in saturated Pt concentration are balanced by the deposition of dissolved material on particles. In electrochemical environment at high voltages, however, the saturated concentration (23)

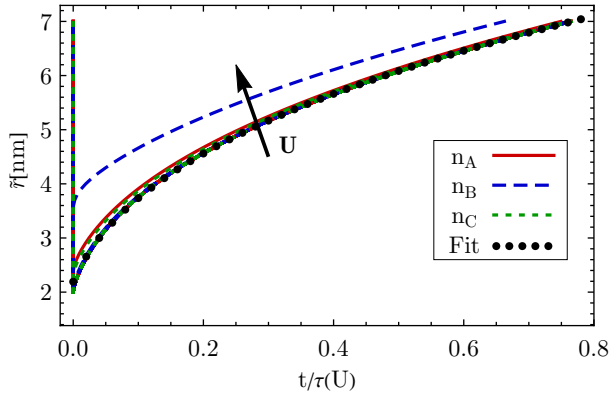

Figure 1: The increase of mean particle size $\bar{r}$ as a function of dimensionless time $t' = t/\tau(U)$ for voltage in range of 0 to 1.4 V in intervals of 0.05 V, and for particle densities $n_A = 2.4 \times 10^{24}/\text{m}^3$, $n_B = 2.4 \times 10^{19}/\text{m}^3$ and $n_C = 2.4 \times 10^{14}/\text{m}^3$. At low voltages, the growth follows power law (21), typical for Ostwald ripening. The best fit function is plotted as a black dotted line.

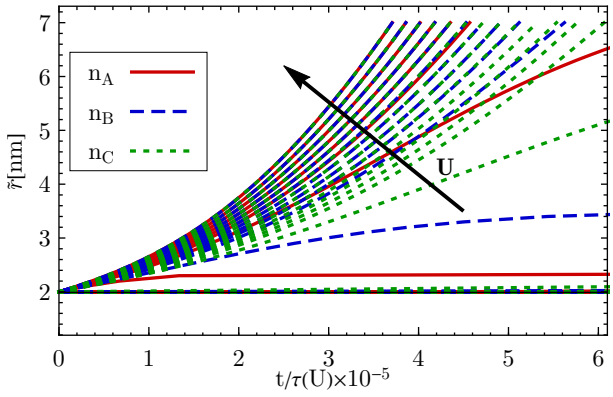

Figure 2: The increase in mean particle size as a function of renormalized time t' for small values of $t' = t/\tau(U)$ for voltage in range of 0 to 1.4 V in intervals of 0.05 V, and for particle densities $n_A = 2.4 \times 10^{24}/\text{m}^3$, $n_B = 2.4 \times 10^{19}/\text{m}^3$ and $n_C = 2.4 \times 10^{14}/\text{m}^3$. The systems at sufficiently high voltage U exhibit an exponential growth of particles for all particle densities.

can be so high that, according to the model, the amount of Pt dissolved in the interparticle space highly exceeds the amount of Pt present in form of particles. In this conditions, the increase in mean particle size, resulting in the lowering of saturated concentration, cannot be balanced by the decrease of Pt ion concentration since the rate of Pt redeposition on particles is insignificant compared to the total amount of total dissolved Pt. The increasing particle size leads to further increase in oversaturation, faster Pt redeposition and consequent exponential particle growth.

The exponential growth can be qualitatively explained if constant Pt concentration (23), not affected by the particle growth, is assumed for the system of uniform particles of size $\bar{r} = r_0$. The equation for particle growth rate in renormalized time t' (12) can for small changes in particle size $\delta r(t') = r(t') - r_0$ be approximated as

$$\frac{\delta r(t')}{dt'} = \frac{r_K^2}{r_0^2} K_r(r_0)\delta r(t'). \tag{24}$$

This results in exponential growth of particles $\delta r(t') \propto \exp \lambda t'$ with exponent $\lambda = \frac{r_K^2}{r_0^2} K_r(r_0)$ being independent of voltage U. It is important to note that this result is applicable only if constant concentration $c_{Pt^{2+}}$ is assumed, which is the case only when the particle density in the system is to low to be able absorb the exceeding amount of dissolved Pt ions.

Although this simple analysis explains the system behaviour on a qualitative level, the fitting of the results of numerical analysis show a linear increase of exponent with voltage $\lambda(U) \approx 3300 + 28000\,\mathrm{V}^{-1} \times U$ and much larger values as predicted by equation (24), for initial state $r_0 = 2\,\mathrm{nm}$ predicting the exponent $\lambda \approx 40\,\mathrm{s}^{-1}$. This discrepancy is probably caused by the effects of finite spread of PSD, with larger particles growing much faster due to larger difference between their equilibrium concentration and actual Pt ion concentration in the system.

Both Figure 2 and the explanation of exponential particle growth by Pt oversaturation suggest that the transition voltage from Ostwald to exponential growth regime depends on the particle density of the system. This assumption is further explored by plotting the renormalized time $t' = t/\tau(U)$, needed for the mean particle size $\bar{r}$ to grow above the characteristic size r_K, as a function of voltage U, shown in Figure 3. We see a sharp drop in growth time when the system transits to exponential growth regime at sufficiently high voltage, which indeed depends on particle density n (solid lines in Figure 3).

To further confirm the proposed explanation based on dissolved Pt oversaturation, the predicted transition voltages were calculated based on few simple assumptions. As a limiting case it was assumed that the initial mass

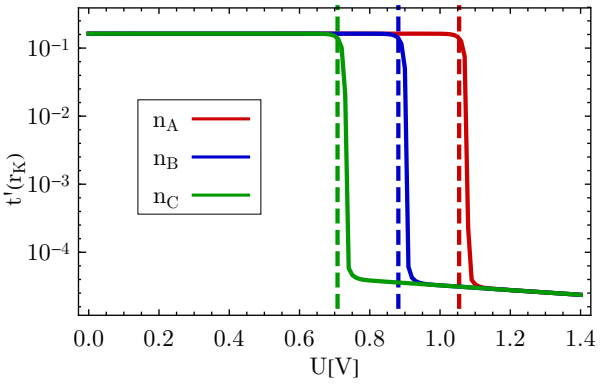

Figure 3: Renormalized time t' needed for the system to reach mean particle size $\bar{r} = r_K$, as a function of electric potential U for particle densities $n_A = 2.4 \times 10^{24}/\mathrm{m}^3$, $n_B = 2.4 \times 10^{19}/\mathrm{m}^3$ and $n_C = 2.4 \times 10^{14}/\mathrm{m}^3$. The transition voltage U_{tr} depends on particle density n, supporting the explanation that the exponential growth occurs when the mass of dissolved Pt in saturated solution m_{dis} significantly exceeds the mass of solid Pt in form of particles m_{sol}. Transition voltages U_{tr}, calculated under assumption $m_{sol} = m_{dis}$, are marked by dashed lines.

of dissolved platinum $m_{dis} = c_S V_0 M$ is comparable to the mass of solid Pt in form of particles, $m_{sol} \approx 4\pi r_0^3 \rho N$, with N being the total number of particles in the system. By equating $m_{dis} = m_{sol}$, expressing particle density as $n = N/V$ and calculating the saturated Pt concentration numerically from (15), the transition voltage U_{tr} between both regimes can be determined:

$$U_{tr} = E_{dis} + \frac{RT}{2n_e\alpha} \log\left[\frac{4\pi r_0^3 n\rho}{3MF[f(r)]}\right]. \tag{25}$$

We see that the transition voltage U_{tr} indeed increases with particle density n. The values of U_{tr}, calculated by numerical integration of $F[f(r)]$ (15) for particle densities n_A, n_B and n_C, are plotted in Figure 3 as solid vertical line for each. The results show a good agreement between predicted and observed transition voltage, further indicating the validity of proposed explanation of exponential particle growth.

Despite sound and plausible interpretation of exponential growth, the actual relevance of this effect in real fuel cell systems is highly questionable. As explained, the process is observed only when the amount of dissolved Pt in initial state exceeds the amount of solid Pt, which is a highly unrealistic situation. Nevertheless, a very similar situation might be present in the fuel cell catalyst during a fast decrease of voltage, when the amount of dissolved Pt strongly exceeds the equilibrium concentration and fast Pt redeposition takes place. However, as seen in Figure 3, the dynamics during exponential growth take place on a

time scale of $10^{-5}\tau(U)$, where the effects of Pt diffusion might play a much more prominent role and should therefore be included in the model. Furthermore, the mean field approach (24), assuming a uniform distribution $c_{Pt^{2+}}$ of dissolved Pt, might be unjustified, calling for additional improvements of the existing models. The results therefore indicate that the system behaviour at high voltages, often found in fuel cells, calls for more refined approach to Pt dissolution to describe the effects not covered in mean field approach typically used in fuel cell degradation models [16, 18].

3.3 Particle size distribution

In this section we will present the properties of PSD $f(r)$ during time evolution in electrochemical Ostwald ripening regime, calculated numerically as explained in Section 2.4, and compare them with the results of LSW theory, presented in Section 2.1. This will be done by comparing the moments of distribution function, namely standard deviation σ and skewness λ, defined as [22]

$$\sigma = \left\langle (r-\bar{r})^2 \right\rangle^{\frac{1}{2}}, \quad \lambda = \frac{\left\langle (r-\bar{r})^3 \right\rangle}{\sigma^3}, \tag{26}$$

where average value is defined as $\langle y(r) \rangle = \int y(r) f(r) dr$ and $\bar{r} = \langle r \rangle$. Note that with this definition, the standard deviation is expressed in units of length while skewness is dimensionless.

It follows from the scaling properties of PSD (5) that the standard deviation of LSW distribution increases linearly with mean particle size and that skewness is constant, with values calculated from (6):

$$\sigma \approx 0.215\bar{r}, \quad \lambda \approx -0.92. \tag{27}$$

Relatively small standard deviation and large negative skewness are typical characteristics and a common point of criticism of LSW solution, since more symmetric and broader distributions are usually observed in experiments [5].

The properties, listed in (27), are compared with numerical results for electrochemical Ostwald ripening by plotting σ and λ as a functions of mean particle size $\bar{r}$ for all three particle densities at voltage levels between 0 and 1.4 V in intervals of 0.05 V. In Figure 4, the standard deviation is plotted as solid lines for voltages below the values U_{tr} (25), dotted for U slightly above U_{tr}, and as dashed line for $U > U_{tr}$. It is clear from the plot that for $U < U_{tr}$, the system obeys linear scaling relation between σ and $\bar{r}$, marked by orange dotted line. Compared to LSW relation (black dotted line), the factor of proportionality is larger, namely $\sigma \approx 0.30\bar{r}$.

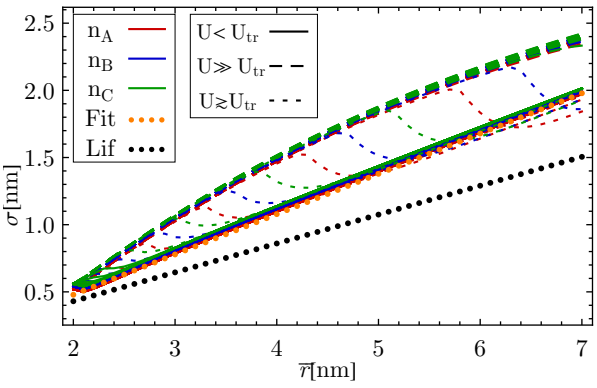

Figure 4: Standard deviation of PSD σ, plotted as a function of mean particle size $\bar{r}$ during system evolution at particle densities $n_A = 2.4 \times 10^{24}/\mathrm{m}^3$, $n_B = 2.4 \times 10^{19}/\mathrm{m}^3$ and $n_C = 2.4 \times 10^{14}/\mathrm{m}^3$ for voltages between 0 and 1.4 V. Two distinct relations between named quantities can be observed, relating to Ostwald ripening growth (linear, solid lines) for voltages $U < U_{tr}$ and to exponential growth regime (dashed lines) at $U \gg U_{tr}$. Systems at voltages only slightly above U_{tr} (dotted lines) transit during evolution from exponential growth regime into Ostwald ripening regime. The results for electrochemical Ostwald ripening show linear dependence between σ and $\bar{r}$ (orange dots), similar to LSW theory (black dots).

Above the transition voltage U_{tr}, the relation between σ and $\bar{r}$ is no longer linear, but interestingly, the relation is still independent of either voltage or particle density, indicating fundamentally the same growth mechanism for all voltages $U > U_{tr}$.

It is interesting to observe that at certain conditions with $U \gtrsim U_{tr}$ (dotted line), the system starts in exponential growth regime, but once the sufficient amount of Pt is redeposited, transits to the Ostwald ripening regime. We see that the relation between σ and $\bar{r}$ after transition to Ostwald regime is practically identical for all systems, regardless of the growth regime at the start of system evolution. This is very important observation, indicating the stability and robustness of the PSD during Ostwald ripening, independent of initial conditions of the system. This property of the observed system will be further highlighted in Section 3.4.

Similarly as in case of standard deviation, the skewness λ exhibits different behaviour in different growth regimes, as seen in Figure 5. What is interesting is that λ is changing with the growth in particle size, which is in contrast with predictions of standard Ostwald ripening theory (27), where constant negative λ is predicted. What is even more surprising is that the sign of skewness in Ostwald ripening regime at $U < U_{tr}$ is positive, which is opposite to the LSW result, where the size distribution is character-

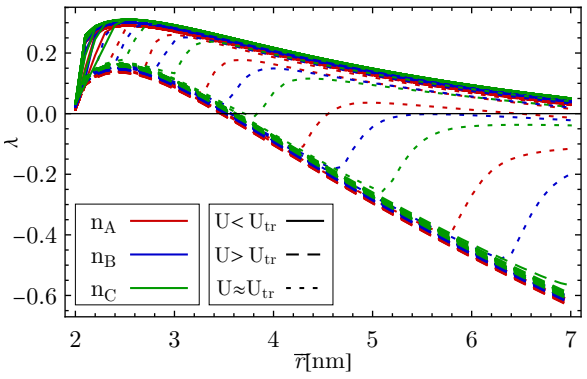

Figure 5: Skewness of PSD λ, plotted as a function of mean particle size $\bar{r}$ during system evolution at particle densities $n_A = 2.4 \times 10^{24}/\mathrm{m}^3$, $n_B = 2.4 \times 10^{19}/\mathrm{m}^3$ and $n_C = 2.4 \times 10^{14}/\mathrm{m}^3$ for voltages between 0 and 1.4 V. Similarly as for standard deviation, the relation between quantities is different for Ostwald ripening regime (solid line, $U < U_{tr}$) and exponential growth regime (dashed line, $U \gg U_{tr}$), with systems transferring from exponential towards Ostwald ripening regime (dotted line, $U \gtrsim U_{tr}$) at sufficiently low Pt oversaturation.

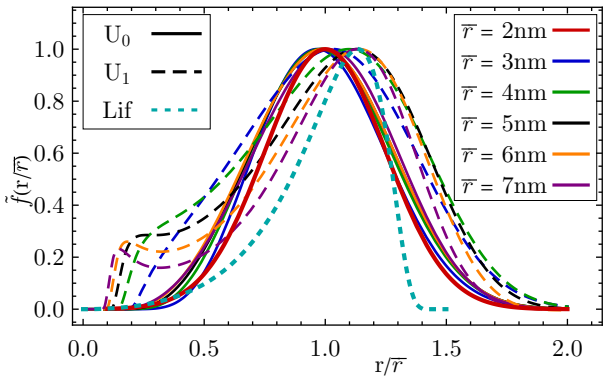

Figure 6: Normalized PSD $\tilde{f}(r)$, plotted as a function of reduced size $r/\bar{r}$ for various values of mean particle size $\bar{r}$ during Ostwald ripening (solid line) and exponential growth (dashed line) system evolution. The distribution during exponential growth shows much more pronounced negative skewness due to fast deposition of Pt on large particles, promoting their growth and skewing the distribution towards the right. The distribution during Ostwald ripening is more symmetric and does not change significantly during system evolution. The distribution is compared with LSW result [6], showing smaller standard deviation σ and more pronounced skenwess λ.

ized by strong negative skewness. The results is important since negative skewness is often used as an indication of Ostwald ripening in the analysis of experimentally measured PSDs, which might lead to incorrect interpretation of growth mechanism in fuel cell catalyst [27]. The experimental measurements on aged fuel cell catalyst samples [26], however, typically show positive skewness, confirming the validity of the modelled results.

Similarly as in the plot of standard deviation σ, we see the systems with $U \gtrsim U_{tr}$ starting in exponentially growth regime evolving gradually to stable Ostwald growth regime if the level of initial oversaturation is sufficiently low (dotted line in Figure 5).

As seen in Figure 5, the skewness of the size distribution in exponential growth regime is changing a sign from positive to negative value during growth. This processes is highlighted in Figure 6 by plotting the scaled PSD at several mean particle sizes between 2 and 7 nm as a function of particle size, scaled by mean size: $r/\bar{r}$. To preserve the transparency, only the results for particles density n_A will be plotted at two different voltages, below transition voltage at $U_0 = 0.4$ V (solid lines), and above U_{tr} at $U_1 = 1.4$ V (dashed line). To simplify the comparison of the results, all distributions are scaled to have the same maximal value, $\tilde{f}(r) = f(r)/\max\left[f(r)\right]$.

As expected, the shape of PSD is significantly different in different growth regimes. In Ostwald growth regime at U_0 (solid line in Figure 6), the shape of the function does not change significantly during growth, which is expected behaviour during Ostwald ripening. For high voltage U_1, on the other hand, the skewness of the distribution is much more significant, evolving from positive towards negative value (dashed line in Figure 6). Especially interesting is a local peak in distribution, emerging at small particle sizes. This is explained by fast deposition of Pt on large particles and slow dissolution of small particles in highly oversaturated environment, resulting in broader distribution with small left-over particles, being dissolved only after the Pt concentration decreases sufficiently. Numerically calculated distributions are further compared to the LSW result (Eq. (6)), plotted as a cyan dotted line in Figure 6. As already explained, the analytic results is much more skewed and narrower than numerically calculated distributions in either electrochemical Ostwald ripening or exponential growth regime.

The experimentally measured PSD, e.g. [26, 28], show more resemblance to results, obtained numerically in this study, than to highly skewed LSW result. Note, however, that in real fuel cell systems the particle size redistribution is affected by competing processes of Ostwald ripening and particle agglomeration, both of which happen simultaneously and at similar conditions [29]. It is therefore difficult to directly compare the results of this study to the experimental measurements, and similar analysis, focused

on particle agglomeration, will be needed to further highlight the combined effect of both processes.

3.4 Effects of initial conditions

As seen in Figures 4 and 5 for the systems just above the transition voltage U_{tr} (dotted lines, $U \gtrsim U_{tr}$), even though initially in exponential growth regime, the transition to Ostwald ripening regime might occur after sufficient time, with system retaining standard relations between standard deviation, skewness and mean particle size. This behaviour supports the argument, given in LSW theory [6], that the asymptotic behaviour of the PSD undergoing Ostwald ripening is universal and independent of initial conditions [5].

To further test this assumption in electrochemical system, the Ostwald ripenign of the system was modelled with with several different initial PSDs with initial mean size between 2 and 5 nm and standard deviations between 0.5 and 1.25 nm, and with particle density n_A. The evolution of each initial state in Ostwald ripening regime at $U = 0.4$ V is presented as a $\sigma - \bar{r}$ plot in Figure 7. It is clear from the plot that the system evolves towards the same linear relation between mean particle size and standard deviation, regardless of initial PSD.

These results confirm that the LSW assumption of universal asymptotic behavior also holds for Ostwald ripening in electrochemical systems. This establishes the relations between mean particle size, standard deviation and skewness, presented in Section 3.3, as a general and universal result in asimptotic limit $t \to \infty$, independent of detailed properties of initial PSD.

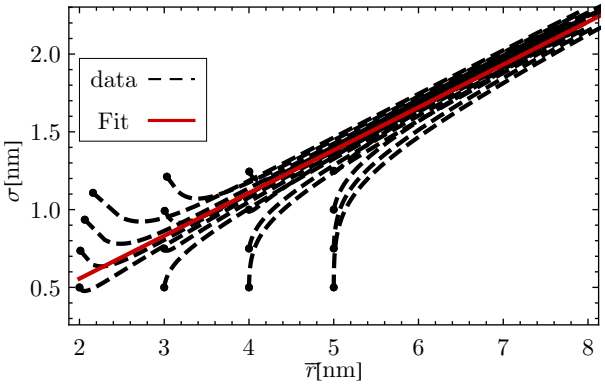

Figure 7: Standard deviation of PSD σ, plotted as a function of mean particle size $\bar{r}$ during system evolution from various initial distributions at voltage $U = 0.4$ V and particle density $n_A = 2.4 \times 10^{24}/\text{m}^3$ (dashed black lines). The convergence of lines towards the same linear relation (red solid line) indicates the robustness and stability of PSD during Ostwald ripening and the generality of the results.

4 Conclusion

The paper systematically analyses the differences between the properties of classical diffusion driven Ostwald ripening and Ostwald ripening in the fuel cell catalyst layer. The analysis relies on numerical integration of governing equations for particle size redistribution, obtained from existing models of fuel cell catalyst degradation. The results were calculated at temperature, electric potential range and initial particle size distribution typical for low temperature fuel cell during its operation. Analysis of results is based on the time dependence of mean particle size and the relations between moments of particle size distribution, namely mean particle size, standard deviation and skewness.

Presented results clearly highlight several important differences between diffusion driven and electrochemically based models of Ostwald ripening, originating primarily from differences in mass transfer mechanism and different characteristic size of the particles. At low potentials, the time dependence of mean particle size in electrochemically driven Ostwald ripening shows similar functional dependence as in diffusion driven process, with growth rate exponentially depending on electric potential. The standard deviation and skewness analysis indicates broader and more symmetric particle size distribution in case of electrochemically driven Ostwald ripening compared to diffusion driven process. Furthermore, the results show that the particle size distribution converges towards the same shape regardless of its initial properties. More importantly, the modelled results at high electric potentials show exponential growth of particles with time, driven by redeposition of platinum from a highly oversaturated solution, which is not observed in the experiments. This indicates severe deficiencies of existing models of fuel cell catalyst degradation to properly describe the Ostwald ripening, originating from poorly implemented modeling of platinum diffusion between catalyst particles.

The presented analysis thus clearly indicates that despite a vast amount of literature dedicated to the study of Ostwald ripening, the modelling approaches for its application in electrochemical devices such as fuel cells, are still not sufficiently developed. Additional research in this field, aimed at improving the treatment of diffusion process in the models of catalyst degradation, will therefore

be needed in the future. This will potentially provide a better understanding and distinction between different catalyst degradation processes in electrochemical devices and enable more efficient development of suitable mitigation strategies.

Acknowledgement: The research is partially funded by Slovenian Research Agency (research core funding No. P2-0401) and by Austrian Research Promotion Agency (research project no. 854867: SoH4PEM).

References

[1] Dubau L., Castanheira L., Maillard F., Chatenet M., Lottin O., et al., A review of PEM fuel cell durability: materials degradation, local heterogeneities of aging and possible mitigation strategies, WIREs Energy Environ.,2014, 3(6) 540–560.
[2] Thomas C.E., Fuel cell and battery electric vehicles compared, Int. J. Hydrog. Energy,2009, 34(15) 6005–6020.
[3] Jain S., Kumar L., Fundamentals of Power Electronics Controlled Electric Propulsion, In Power Electronics Handbook, 4th edition, (Elsevier, 2018), 1023–1065.
[4] Ostwald W., Z. Phys. Chem, 1901, 37 385.
[5] Baldan A., Review progress in Ostwald ripening theories and their applications to nickel-base superalloys Part I: Ostwald ripening theories, J. Mater. Sci, 2002, 37(11) 2171–2202.
[6] Lifshitz I.M., Slyozov V.V., The kinetics of precipitation from supersaturated solid solutions. J. Phys. Chem. Solids, 1961, 19(1-2) 35–50.
[7] Wagner C.W., Theory of the aging of precipitates by dissolution-reprecipitation Zeitschrift für Elektrochemie, 1961, 65 581.
[8] Ardell A.J., The effect of volume fraction on particle coarsening: theoretical considerations, Acta Met., 1972, 20(1) 61–71.
[9] Brailsford A.D., Wynblatt P., The dependence of ostwald ripening kinetics on particle volume fraction, Acta Met., 1979, 27(3) 489–497.
[10] Davies C.K.L., Nash P., Stevens R.N., The effect of volume fraction of precipitate on Ostwald ripening, Acta Met., 1980, 28(2) 179–189.
[11] Marqusee J.A., Ross J., Theory of Ostwald ripening: Competitive growth and its dependence on volume fraction, J. Chem. Phys, 1984, 80(1) 536–543.
[12] Slezov V.V., Sagalovich V.V., Tanatarov L.V., Theory of diffusive decomposition of supersaturated solid solution under the condition of simultaneous operation of several mass-transfer mechanisms, J. Phys. Chem. Solids, 1978, 39(7) 705–709.
[13] Myers T.G., Fanelli C., On the incorrect use and interpretation of the model for colloidal, spherical crystal growth. J. Colloid Interface Sci., 2019, 536(2019) 98–104.
[14] Alexandrov D.V., On the theory of Ostwald ripening in the presence of different mass transfer mechanisms, J. Phys. Chem. Solids, 2016, 91 48–54.
[15] Alexandrov D.V., On the theory of Ostwald ripening: formation of the universal distribution. J. Phys. A, 2015, 48(3) 035103.
[16] Darling R.M., Meyers J.P., Kinetic Model of Platinum Dissolution in PEMFCs, J. Electrochem. Soc, 2003, 150(11) A1523.
[17] Darling R.M., Meyers J.P., Mathematical Model of Platinum Movement in PEM Fuel Cells. J. Electrochem. Soc, 2005, 152(1) A242.
[18] Rinaldo S.G., Lee W., Stumper J., Eikerling M., Model- and Theory-Based Evaluation of Pt Dissolution for Supported Pt Nanoparticle Distributions under Potential Cycling. Electrochem. Solid-State Lett, 2011, 14(5) B47.
[19] Rinaldo S.G., Urchaga P., Hu J., Lee W., Stumper J., Rice C., Eikerling M., Theoretical analysis of electrochemical surface-area loss in supported nanoparticle catalysts. Phys. Chem. Chem. Phys, 2014, 16(48) 26876–26886.
[20] Urchaga P., Kadyk T., Rinaldo S.G., Pistono A.O., Hu J., Lee W., Richards C., Eikerling M., Rice C., Catalyst Degradation in Fuel Cell Electrodes: Accelerated Stress Tests and Model-based Analysis. Electrochim. Acta, 2015, 176 1500–1510.
[21] Kregar A.,Tavčar G., Kravos A., Katrašnik T., Predictive virtual modelling framework for performance and platinum degradation modelling of high temperature PEM fuel cells. Energy Procedia, 2019, 158 1817–1822.
[22] Joanes D.N., Gill C.A., Comparing measures of sample skewness and kurtosis. J. Royal Stat. Soc: Series D (The Statistician), 1998, 47(1) 183–189.
[23] Jayasankar B., Karan K., O_2 electrochemistry on Pt: A unified multi-step model for oxygen reduction and oxide growth. Electrochim. Acta, 2018, 273 367–378.
[24] Darab M., Barnett A.O., Lindbergh G., Thomassen M.S., Sunde S., The Influence of Catalyst Layer Thickness on the Performance and Degradation of PEM Fuel Cell Cathodes with Constant Catalyst Loading. Electrochim. Acta, 2017, 232 505–516.
[25] Ames W., Numerical Methods for Partial Differential Equations, 3 edition (Academic Press, 2014).
[26] Ferreira P.J., la O' G.J., Shao-Horn Y., Morgan D., Makharia R., Kocha S., Gasteiger H.A., Instability of Pt/C Electrocatalysts in Proton Exchange Membrane Fuel Cells. J. Electrochem. Soc., 2005, 152(11) A2256.
[27] Vion-Dury B., Chatenet M., Guétaz L., Maillard F., Determination of Aging Markers and their Use as a Tool to Characterize Pt/C Nanoparticles Degradation Mechanism in Model PEMFC Cathode Environment. *ECS Transactions*, 2011, 41(1) 697–708.
[28] Rasouli S., Ortiz Godoy R.A., Yang Z., Gummalla M., Ball S.C., Myers D., Ferreira P.J., Surface area loss mechanisms of Pt_3Co nanocatalysts in proton exchange membrane fuel cells. J. Power Sources, 2017, 343 571–579,.
[29] Jahnke T., Futter G., Latz A., Malkow T., Papakonstantinou G. et al., Performance and degradation of Proton Exchange Membrane Fuel Cells: State of the art in modeling from atomistic to system scale. J. Power Sources, 2016, 304 207–233.